Predictive modelling of seabed habitats: Case study of subtidal kelp forests on the coast of Brittany, France

Article *in* Marine Biology · July 2010

DOI: 10.1007/s00227-010-1426-4 · Source: OAI

Marine Biology
July 2010, Volume 157, Number 7, Pages 1525-1541
http://dx.doi.org/10.1007/s00227-010-1426-4

The original publication is available at http://www.springerlink.com

Predictive modelling of seabed habitats: case study of subtidal kelp forests on the coast of Brittany, France

Vona Méléder[1, 3, *], Jacques Populus[1], Brigitte Guillaumont[1], Thierry Perrot[2] and Pascal Mouquet[2]

[1] Ifremer, Dyneco/AG, BP 70, 29280 Plouzané, France
[2] CEVA, BP 3, L'Armor-Pleubian, 22610 Pleubian, France
[3] Present address: Nantes Atlantique Université, Mer Molécule Santé/EA 21 60, BP 92208, 44322 Nantes cedex 3, France

*: Corresponding author : Vona Méléder, email address : vona.meleder@univ-nantes.fr

Abstract:

Predictive modelling to map subtidal communities is an alternative to "traditional" methods, such as direct sampling, remote sensing and acoustic survey, which are neither time- nor cost-effective for vast expanses. The principle of this modelling is the use of a combination of environmental key parameters to produce rules to understand species distribution and hence generate predictive maps. This study focuses on subtidal kelp forests (KF) on the coast of Brittany, France. The most significant key parameters to predict KF frequency are (1) the nature of the substrate, (2) depth, (3) water transparency, (4) water surface temperature and (5) hydrodynamics associated with the flexibility of algae in a flow. All these parameters are integrated in a spatial model, built using a Geographical Information System. This model results in a KF frequency map, where sites with optimum key parameters show a deeper limit of disappearance. After validation, the model is used in the context of Climate Change to estimate the effect of environmental variation on this depth limit of KF. Thus, the effects of both an increase in water temperature and a decrease in its transparency could lead to the complete disappearance of KF.

INTRODUCTION

Traditionally, marine ecologists have used the direct sampling method to characterise shallow water and intertidal marine habitats. However, this method is neither time- nor cost effective for expanses from a regional to a global scale. Remote sensing tools, such as aerial photography, airborne and satellite imagery, are appropriate for surveying and classifying marine habitats in the intertidal zone (Guillaumont et al. 1993; Bajjouk et al. 1996; Guillaumont et al. 1997; Méléder et al. 2003; Combe et al. 2005). However, these tools rapidly reach their limits for subtidal surveys because of the absorption of visible radiations by water. Both single-beam and sidescan acoustic methods are suitable to overcome this limitation and to achieve remote sensing of depth and benthic communities in subtidal waters (McRea et al. 1999; Piazzi et al. 2000; Brown et al. 2002; Freitas et al. 2003; Riegl et al. 2005; Freitas et al. 2006). But as these techniques involve either profiles or narrow swaths, their efficiency of coverage is quite limited and addressing areas from regional to global scale leads to dramatically increased costs. Acoustic methods also have limited discriminatory ability between macrophyte types and densities although recent works show their capability to coarse estimate macrophytic biomass (Riegl et al. 2005). So, for spatial assessment of seabed habitats, prediction using models seems to be the best approach. Depending of the objective of the survey and the availability of data to build models, assessment could include the occurrence, the biomass, the density and/or the diversity of habitats. Although these tools cannot replace direct detection or observation of benthic surfaces, they can provide a more global vision of some seabed habitats that is compatible with ecosystem management. The development of predictive models will contribute to better understanding of the factors and processes which structure the distribution and composition of marine habitats and their associated biological communities at a coarser yet more integrated scale than that achieved using direct methods. Once developed and validated, these models are time- and cost-beneficial tools and enable the coverage of areas where no habitat information is available. Besides, they offer a way to apply scenarios to simulate effects of environmental changes on habitats distribution, particularly in the contemporary context of the Climate Change (IPCC 2001).

Some combinations of environmental parameters, such as the so-called the 'marine landscape', are assumed to control the distribution of species and habitat types (Roff and Taylor 2000). Basically, the key parameters used can be grouped under three themes (Stevens and Connolly 2004), i.e., those concerned with 1/ the morphology of the bottom and the nature of the substrate (depth, sediment type, sediment constituents), 2/ the nature of the water body overlying the substrate (temperature, pH, salinity, turbidity, nutrients) and 3/ the dynamics of the local environment or water mass (exposure to waves, current velocity). Since the approach proposed by Roff & Taylor in 2000 to predict the distribution of species and habitat types using 'marine landscapes', there have been a few examples of marine habitat classification in a spatial context based on physical factors (Zacharias et al. 1999; Kelly et al. 2001; Zacharias and Roff 2001; Brinkman et al. 2002; Stevens and Connolly 2004; Greve and Krause-Jensen 2005; De Oliveira et al. 2006). Applied to a marine context, these methodologies are expected to produce rules to understand species distribution according to environmental parameters and hence, predictive maps.

The aim of this study, part of a modelling work package of the MESH project (Mapping European Seabed Habitats), an Interreg IIIB North-West Europe funded initiative, is to propose a predictive model of kelp forest (hereafter called KF) frequency, i.e., the percentage of their presence along the coast of Brittany, France. Indeed, seaweeds are an important component of coastal primary production. With a primary production ranging from 400 to 1900 g $C.m^{-2}.y^{-1}$ (Sivertsen 1997), KF can be compared to the most productive terrestrial ecosystems (Hurd 2000). Characterised by densities of more than <u>3 plants.m^{-2}</u> and made up of various seaweed species belonging to the Laminariales order, essentially *Laminaria digitata* and *Laminaria hyperborean*, KF are often the dominant producers in nearshore ecosystems, supplying higher trophic levels via herbivory or the detrital food chain (Hurd 2000 and references within). KF also provide an essential habitat and food for hundreds of marine invertebrates and fish species living in temperate nearshore waters (Norderhaug et al. 2002 <u>and references within</u>). However, they also react to changes in environmental <u>changes and/or quality</u> (Dayton et al. 1992; Ferrat et al. 2003). Finally, KF are used in many maritime countries for industrial applications and as a fertiliser. This means that there is a steady demand for raw material from the seaweed industry, adding economic importance to their ecological one.

In this current study, KF frequency is predicted as a function of the depth and the chosen methodology for the prediction is the stepwise multiple regression process with a backward selection of environmental variables: water transparency, temperature and water motion. The software used to build and validate the model and to display the resulting map is a Geographical Information System (GIS), ArcGIS 9.0. After validation, model is used in the context of Climate Change to estimate the effect of environmental variation on KF distribution.

MATERIALS AND METHODS

Environmental variables

Nature of substrate – As KF are mainly found on rocky substrata, the prediction of their occurrence was limited to this kind of substrate. Thus, maps of rock in shapefile format were used as masks to force the model in the GIS software, namely digital sediment maps (SHOM 1994-2005) with a resolution of 1:50,000 and where not available, a coarser 1:500,000 map (Vaslet et al. 1979).

Bathymetry – The bathymetry map was a raster dataset from the French Channel coast to the Gironde estuary, with a resolution of 150 m. This raster was generated using various types of digital and map depth data that were interpolated by kriging, a geostatistical method. Bathymetry was expressed in metres with respect to the LAT (lowest astronomical tide level). However, this depth did not correspond to the real water column height, since LAT levels are rarely reached. Therefore, depth values were locally corrected by the annual mean tide level, leading to a new raster dataset of water column height to be used as an input for the predictive model. For the sake of simplicity, this water height will be called "depth" in the paper.

Another bathymetric derivative was also calculated, the BPI (Bathymetric Position Index, Lundblad et al. 2004). This index enabled the topography to be estimated (crest / depression / flat or slope) by measuring where a given depth cell was located with regard to the overall landscape. In the present case the mean depth of the surrounding cells was computed using a 4 cell radius annulus. The cells in the resulting raster dataset were assigned values within a range of positive and negative numbers. A positive BPI indicated a cell on a crest, whereas a negative index was found where a depression occurred. Flats areas or areas with a constant slope produced index values near zero (Lundblad et al. 2004).

Water transparency – In coastal waters, light is very often a key limiting factor for the growth of photosynthetic organisms such as the laminarial algae constituting KF, and the light attenuation coefficient in the euphotic layer is a major parameter used in ecological modelling. Thus, the attenuation coefficient of the photosynthetically available radiation (PAR domain [400 – 700 nm]), K_{PAR} enabled the light attenuation throughout the water column to be modelled. This coefficient, derived from the water optically active components related to chlorophyll, suspended particulate matter and dissolved organic matter could be used as a water turbidity proxy. Hence, a high attenuation coefficient illustrates a turbid water column. In this study, K_{PAR} was derived from SeaWiFS (Sea Wide Field Sensor) satellite reflectance, combining chlorophyll and suspended matter optical properties (Gohin et al. 2005). 52 weekly mean images of K_{PAR} were obtained from SeaWiFS data averaged over the 1998-2004 period, with a resolution of 1,100 m.

From this K_{PAR} the fraction of light reaching the bottom (Fr) was estimated for a given depth h by:

$$Fr = (\exp^{h \times K_{PAR}}) \times 100 \ (\%) \qquad (1)$$

When this percentage is equal to 1%, it defines the lower limit of the photic zone. Below this threshold, the remaining energy is not efficient for photosynthesis.

Temperature – This factor was estimated by Sea Surface Temperature (SST, in °C) derived from AVHRR (Advanced Very High Resolution Radiometer) data with a resolution of 1,100 m. SST maps were provided by the SAF (Satellite Application Facility) “Ocean and Sea Ice” of EUMETSTAT/Meteo-France, Lannion (France) and 52 weekly mean images were available from AVHRR reflectance averaged over the last two decades.

Water motion – This variable was expressed as the tidal current maximum velocity (Vmax in $m.s^{-1}$) resulting from simulations for a mean spring tide run by the hydrodynamic model MARS 3D developed at Ifremer. The current resolution of this model is 300 m.

Biological variables: KF ground-truthing

Acoustic surveys of laminarial algae belonging to KF were carried out at 10 locations along the Coast of Brittany in three periods: spring 2005 for the Aber Wrac'h (AW) site, spring 2006 for the Groix (Gr), Molène (Mo), Méloine (Me) and Triagoz (Tr) sites and spring 2007 for the Audierne (Au), Bréhat Island (Br), Glénan (Gl), Heaux (He) and Moelan (Ml) sites (Figure 1). All sites were chosen for the presence of rocky substrata and the accessibility to survey boat. Prospected zone for each site was delimited using rock and bathymetry maps to identify flat rocky area located at a bathymetry varying from 10 to 30 m, where KF were more susceptible to be found. On field, a small survey boat equipped with a 120 kHz Simrad EK60 echo-sounder was used. The narrow 7° width beams were used for emitting and receiving. The acquisition parameters of the transducer, adjusted to the minimum pulse duration (64 µs) and sampling interval (pulse frequency: 16 µs), made it possible to obtain the maximum resolution on both vertical and horizontal axes. All recordings were performed at a constant speed of about 5 knots corresponding to a distance between each pulse (or ping) varying from 5 to 20 cm. The total track length for each site was about 20 kilometres. Acoustic transects were simultaneously georeferenced with a GPS equipped with the EGNOS system giving position accuracy of better than three metres. Both acoustic and position data were stored on a laptop PC.

Data processing - Raw acoustic data were post-processed using MOVIES+ echo integration software (Marchalot et al. 2003) which can be used to evaluate the backscattered energy in different depth layers defined by the user above or below the seafloor (Figure 2, line A). The first layer was defined at 0.2 m above the sea bottom to detected KF (Figure 2, line B) and the second from 1 to 1.5 m under the sea bottom to evaluate the nature of the seafloor (not shown in Figure 2). The top limit of the integrated layer was set at 2.2 m above the bottom (line C). On each ESU (Elementary Sampling Unit, Figure 2), defined by a 20-ping width and a spatial resolution varying from 1 to 4 m (depending on the speed of the boat), the software gives four parameters for each layer: *Ni* (number of echo-integrated samples), *Nt* (total number of samples), *sA* (nautical area scattering coefficient in the layer in m^2/mille^2) and *sV* (volume reverberation index of the layer in dB). The additional parameter *BotErr* (for Bottom Error), provided by the software when a large variation is detected in the echo-integrated energy, may indicate that the bottom itself has accidentally been integrated in the first bottom layer (i.e., the one nearest the sea bed, see Figure 2, line A). Once the raw acoustic data have been processed using MOVIES+, a specific algorithm implemented with the Excel software based on thresholds and ratio values of *Ni*, *Nt, sA* and *BotErr* automatically classifies KF presence or absence (binary) and the type of substrate (rock or sand). The algorithm was validated using direct observations by scuba-divers on the AW site during spring 2005 and in the Gr, Mo, Me and Tr sites during the spring 2006.

Thus, the resulting data for each ESU were the coordinates of the point (lat, long), the KF presence or absence, the nature of the substratum, and the depth (in metres). The latter, initially measured with reference to LAT, was corrected by adding the annual mean tide level.

The echo-integration results were used to build KF distribution laws, expressed for each site in “percentage of presence” or “frequency” (%) as a function of depth (m). KF frequency, $F_{[H]}$, was obtained for depths between 10 and 30 m by:

$$F_{[H]} = \frac{\sum_{h \geq H-0.25}^{h<H+0.25} KF_H}{\sum_{h \geq H-0.25}^{h<H+0.25} R_H} \times 100 \qquad (2)$$

where H was the class of depth split into 0.5 m intervals and *h* the depth from echo-integration falling into this class, KF_H the total amount of ESU corresponding to KF for the given class H and R_H the total amount of ESU corresponding to rock substratum for the same class H.

These frequency laws were fitted using piecewise regressions (Toms and Lesperance 2003) from SigmaPlot 10.0 software following the process:

$h_1 = \min(h)$

$h_3 = \max(h)$

$\text{segment1}(h) = (y_1 \times (H_1 - h) + y_2 \times (h - H_1)) / (H_1 - h_1)$ (3)

$\text{segment2}(h) = (y_2 \times (H_2 - h) + y_3 \times (h - H_1)) / (H_2 - H_1)$ (4)

$\text{segment3}(h) = (y_3 \times (h_3 - h) + y_4 \times (h - H_2)) / (h_3 - H_2)$ (5)

$f = \text{if } (h \leq H_1 \text{ ; segment1}(h) \text{ ; if } (h \leq H_2 \text{ ; segment2}(h) \text{ ; segment3}(h)))$

The fit was sought for the two breakpoints H_1 and H_2 and $Slope_2$, the slope between them (Figure 3). H_1 and H_2 were the depths corresponding respectively to the beginning of the frequency decrease and to the disappearance of KF, (which is also the upper limit of KF characterised by a density of less than 3 plants.m^{-2}). These three parameters were taken as the biological variables to be predicted using environmental ones. Each fit was expressed with its confidence and prediction intervals at 95 % (Figure 3).

Model building

The cell values of the environmental variable raster dataset (BPI, K_{PAR}, SST and Vmax) intersected by acoustically surveyed transects were extracted and averaged on a site basis. The values from five sites (AW, Mo, Me, Tr and Gr) called “training sites” were used to build the predictive model of KF frequency, whereas the values from the other five (Au, Br, Gl, He and Ml called “validation sites”) were used to validate it.

The methodology chosen for the prediction was the stepwise multiple regression with a backward selection of variables. Associations of the BPI and/or K_{PAR} and/or SST and/or Vmax were used to predict H_1, H_2 and $Slope_2$, and then to estimate KF frequency for depths from H_1 to H_2:

$$H_1 = aBPI + bSST + cK_{PAR} + dVmax^{\beta} \qquad (6)$$

$$H_2 = a'BPI + b'SST + c'K_{PAR} + d'Vmax^{\beta} \qquad (7)$$

$$Slope_2 = a''BPI + b''SST + c''K_{PAR} + d''Vmax^{\beta} \qquad (8)$$

$$\text{Predicted KF frequency (\%)} = Slope_2 \times (h - H_2) \qquad \text{for } H_1 < h < H_2 \qquad (9)$$

where, a to c” were the regression coefficients (might be = 0), and the β exponent expressed the flexibility of algae in a flow, typically around 1.5 (Denny and Gaylord 2002). 2 and 1.5 were tested as values for β.

The prediction of KF frequency for a depth less than H_1 is performed using the same process:

$$\text{Predicted KF frequency (\%)} = wBPI + xSST + yK_{PAR} + zVmax^{\beta} \qquad (10)$$

for $h < H_1$

where w to z are the regression coefficients (might be = 0) and β=1.5 or 2.

Stepwise regressions were run using the statistical software R.2.5.1. However, the use in regression process of the 52 weekly values extracted from K_{PAR} and SST images was not relevant. For this reason, water transparency and surface temperature information were synthesised using both the annual average (namely K_{PAR}year and SSTyear) and the average during the growth period from week 14 to week 25 (namely K_{PAR}growth and SSTgrowth). The minimum and maximum values during the year (K_{PAR}min, SSTmin, K_{PAR}max and SSTmax) were also integrated in the stepwise regression process. Then environmental variables with a non-significant partial F ($p \leq 0.1$) were removed step by step. However, varying significant multiple or simple regressions were obtained to predict the same biological variables. All these regressions were used to build varying predictive models, and the one showing the smallest residual differences between predictions and observations was kept to produce the final predictive map. This map was then built by automating the model work flow with the 'ModelBuilder' interface in the ArcGIS 9.0 geoprocessing toolbox. Moreover, this interface allowed to create the environmental settings for the model, which controlled geoprocessing output parameters. Raster analysis settings were used to give the output cell size, defining working scale, the finest resolution among the various data sources, 150 m, and to apply the rock mask.

Validation and simulations

KF frequency obtained by echo-sounding from the 5 sites: Au, Br, Gl, He and Mo (Figure 1) was compared to the prediction at the same location to validate the model.

It was then used in the context of Climate Change to estimate the effect of environmental variation on the depth of KF disappearance, H_2. Indeed, since 1976, temperature of the ocean increase by 0.075 °C/decade, i.e. an increase of around 0.2 °C during the 30 past years (IPCC 2001). For the northern hemisphere, where this study sites are located, the increase of temperature is higher with 0.4 °C/decade, i.e. around 1 °C since 1976 (IPCC 2001). Using the validated model, two scenarii were tested for temperature increase in accordance to IPCC (2001) results: the global (0.2 °C) and the northern increase (1 °C). An intermediate stage (an increase of 0.5 °C) was used in a third simulation. In the same way, three scenarii to estimate effect of an increase of water transparency on KF distribution were tested. Indeed, extreme episodic events such as storms, extreme rain events and flooding must a consequence of the Climate Change (IPCC 2001). These result in strong hydrodynamics and super river discharges leading to decrease of water transparency (de Jonge and de Jong 2002; Cardoso et al. 2008). However, no information about the evolution of the water transparency proxy use in this study, the K_{PAR}, is available. Steps to simulate increase of K_{PAR} values for the three scenarii were chosen to test K_{PAR} values included in the range of values used to build the model: 0.01, 0.02 and 0.05.

RESULTS

Environmental parameters

Gr, He and Br sites were the more turbid locations throughout the year and during the growth period with the greatest K_{PAR}year and K_{PAR}growth values (Table 1). For these three sites, the minimum values (K_{PAR}min) never went below 0.18, whereas maximum values (K_{PAR}max) reached 0.456 at the Gr site during week 2 (Table 1,

Figure 4). On the other hand, the western sites Mo and Au were the clearest locations with lowest K_{PAR} values (Table 1).
Along with this spatial variability along the coast of Brittany, water transparency also varied over time. Peaks of K_{PAR}, often exceeding 0.25, were detected during the first seven weeks and the last twelve weeks (Figure 4). These periods corresponded respectively to winter and autumn, periods of bad weather with rain and storms often leading to increased amounts of mineral material from either bottom scouring or river discharge. The maximum K_{PAR} values reported in Table 1 were recorded during these weeks. Conversely, the minimum K_{PAR} values (K_{PAR}min, Table 1) were observed during spring/summer between weeks 10 and 40. This period corresponded to calm weather, although some turbulent and stochastic events appeared and generated turbidity peaks lasting from one to three weeks but never resulting in a K_{PAR} above 0.25 (Figure 4). These peaks were essentially observed at AW, Gr, Br and He sites, whereas the other sites were more stable in terms of water transparency (Figure 4).

Surface temperature showed spatial and temporal variability very similar to that of water transparency. The warmest sites during the year were those located in the south: Gr, Gl and Ml with respectively 13.6, 13.7 and 13.5°C (Table 1), which also exhibited growth period temperature values in excess of 12.5°C. The coldest site was AW with more than 1°C below the annual means o f the southern sites. The other sites showed equivalent annual SST values, around 13°C (Table 1).
The temporal variability was classic, with high temperatures in summer, and low temperatures in winter (Figure 5). However the Gr site, although it was one of the warmest, showed the minimum temperature value (8.7° C), due to a well-known

tongue of cold water occurring near the coast. The other southern sites showed the highest minimum and maximum temperature values (Table 1, Figure 5).

Exposure, measured by the maximum tidal current velocity Vmax, showed a north/south gradient whose maximum velocity was lower than 0.3 $m.s^{-1}$ for southern sites, although it reached 1 $m.s^{-1}$ for the more turbulent northern sites (Table 1).

Surveying KF with echo-sounding

The parameters described in the Materials and Methods section were calculated for the echo signals collected over the study areas and the binary classification of KF (presence/absence) was performed for each site. For illustrate results, only part of the echogram for the Gl site and the corresponding classification are shown in Figure 6. The acoustic signal from KF is about 1 metre high with quite low backscatter energy (light grey) above the seafloor (dark grey). There was good correlation between underwater KF boundaries as indicated by the echogram and the classification (dark hatches). Sometimes, accidental bottom integration causes classification of the ESU in *BottErr* (light hatches). This phenomenon is generally seen on steeper rocky substrates and is amplified by bad weather conditions.

KF frequency law

Overall, the sites showed the same significant distribution profile along the depth (Figure 3, Table 2), except for those of Au, He and Ml, for which some fit parameters are not significant (Table 2). The profile was divided in two parts. The first, before the inflexion point H_1, corresponded to the variability of frequency around a mean (Figure 3). The slope of this first segment was not significant, and thus, was not predicted by the model. Indeed, the frequency for depths less than H_1 up to the upper KF limit were directly predicted using environmental parameters (eq. 10). The second part of distribution law corresponded to a drop in the frequency along $Slope_2$, between H_1, and H_2, the depth at which KF disappeared (eq. 4 to 6). Fits are good, with high adjusted R^2 and a probability of less than 0.01 (Table 2). H_1 varies from 13.2 m for the most turbid and coldest site Br, to 20.6 m for the clearest and warmest one, Mo (Tables 1 and 2). Likewise, $Slope_2$ is higher in turbid (low transparency) and cold sites, such as Au and Br, than in less turbid and warmer sites such as Me and AW (Tables 1 and 2). Similarly to H_1 and $Slope_2$, H_2 varies with the water transparency and surface temperature from 19.3 m to 27.8 m. However, the relationship between H_2 and water transparency and/or surface temperature is not as clear as that explaining H_1 and $Slope_2$, suggesting the effect of another environmental parameter to explain explaining KF disappearance, which could be bed stress.

Once H_2 was known, the Fr fraction (eq. 1) for each site was calculated using the four water transparency parameters K_{PAR}year, K_{PAR}gowth, K_{PAR}min and K_{PAR}max (Table 3). Only K_{PAR}growth and K_{PAR}min values allowed Fr higher than the 1% threshold permitting photosynthesis activity. The use of K_{PAR}year and K_{PAR}max generated Fr values below the 1% level which were inconsistent with algal presence such as KF or parks. Thus, only K_{PAR}growth and K_{PAR}min seemed to be relevant and biologically interpretable abiotic factors to predict H_2 and hence KF frequency.

Predictive modelling

Stepwise regression processes provided four significant models to predict KF frequency from the five training sites AW, Mo, Me, Tr and Gr, for a depth ranging from H_1 to H_2 following the equations (6) to (9). The first model predicted biological variables (H_1, H_2 and $Slope_2$) using SSTmin only (eqs. 11 to 13) and the second one used K_{PAR}min only (eqs. 14 to 16). The last two significant models were similar to the first two, but with a better predictive H_2 using $Vmax^{1.5}$ in addition to SSTmin or K_{PAR}min alone (eqs. 17 and 18). The adjusted R^2 increased from 0.80 to 0.98 when $Vmax^{1.5}$ was associated with SSTmin, and from 0.76 to 0.97 when $Vmax^{1.5}$ was associated with K_{PAR}min:

pred_mod1,

$$H_1 = -29.81 + 5.31 \times SSTmin \qquad R^2 = 0.88,\ p \leq 0.05 \quad (11)$$

$$H_2 = -30.32 + 5.86 \times SSTmin \qquad R^2 = 0.80,\ p \leq 0.05 \quad (12)$$

$$Slope_2 = 28.53 - 4.23 \times SSTmin \qquad R^2 = 0.79,\ p \leq 0.05 \quad (13)$$

pred_mod2,

$$H_1 = 40.5 - 121.19 \times K_{PAR}min \qquad R^2 = 0.87,\ p \leq 0.05 \quad (14)$$

$$H_2 = 40.75 - 130.97 \times K_{PAR}min \qquad R^2 = 0.76,\ p \leq 0.05 \quad (15)$$

$$Slope_2 = -25.37 + 84.72 \times K_{PAR}min \qquad R^2 = 0.60,\ p = 0.12 \quad (16)$$

pred_mod3,

H_1 = eq. (14)

$$H_2 = 43.53 - 121.12 \times K_{PAR}min + 2.26 \times Vmax^{1.5} \qquad R^2 = 0.97,\ p \leq 0.05 \quad (17)$$

$Slope_2$= eq. (16)

pred_mod4,

H_1 = eq. (11)

$$H_2 = -26.86 + 5.33 \times SSTmin + 2.07 \times Vmax^{1.5} \qquad R^2 = 0.98,\ p \leq 0.05 \quad (18)$$

$Slope_2$= eq. (13)

For each model, the KF frequency was predicted following equation (9). Thus, the most efficient model was that reducing residuals between observation and prediction (Figure 7). These residuals showed that models including temperature or water transparency only (respectively pred_mod1 and pred_mod2) were not able to predict KF frequency correctly (Figure 7a and 7b). Indeed, SSTmin on its own (pred_mod1) predicted KF frequency well only for the Gr and Me sites, whereas this model overestimated percentages for the sites AW and Mo and underestimated them for Tr (Figure 7a). On the contrary, K_{PAR}min (pred_mod2, Figure 7b) enabled good prediction for the latter site as well as for Me, while it overestimated observations for Mo and underestimated those on AW. The use of water motion, estimating bed stress using $Vmax^{1.5}$, was more efficient (Figure 7c and 7d) particularly when it was associated with water transparency (Figure 7c). Only the observed frequencies from the Gr site were not well predicted using the model 'pred_mod3' but this was due to incomplete coverage by SeaWiFS data for this site. Therefore, the model using SSTmin and $Vmax^{1.5}$ (Figure 7d) was run for part of this site and other locations where water transparency data were not available.

Models were able thus to predict a decrease in depths H_1 and H_2 with water clarity, while an increase in temperature indicated deeper breakpoints. When clearness or surface temperature of water was constant a drop in the depth limit H_2 occurred in a direct ratio with a power of 1.5 for the velocity. Finally, the model providing the best prediction of KF frequency for depths between H_1 to H_2 was pred_mod3, using water transparency and bed stress, or pred_mod4 when water transparency data were not available.

However, the only significant model to predict KF frequency for a depth less than $H_{1,}$ following equation (10) was that using topography (BPI) alone:

$$\text{Predict \%} = 52.5 - 1.64 \times \text{BPI} \qquad R^2 = 0.75,\ p \leq 0.01 \quad (19)$$

This regression indicates that KF were observed preferentially in depressions rather than on crests. But, the attempted validation of this model concluded that using BPI as a physical parameter can correctly predict KF frequency values around 50% (Figure 8). Under or above this frequency, BPI alone did not explain occurrences of KF in well-lit water.

The prediction was stopped at the +1m depth contour, known to be the higher limit of KF presence. It was not possible to predict this limit at the study scale, as was done by De Oliveira (2006) who used the percentage of immersion over the year, derived from the tidal flooding frequency at a given elevation. This limit occurred for KF between immersion periods ranging from 92 to 97 % whereas maximum KF coverage occurred at 100 % immersion. The depth contours corresponding to ~ 95 % and 100 % immersion were too closes (only a few tens of metres), so they were included in the same pixels of the bathymetry dataset used in our model. Therefore, estimating and mapping the decrease in KF frequency between these two contours at our working scale (150 m) was not possible.

Model validation

Validation sites Au, Br, Gl, He and Ml (Figure 1) were used to validate the selected model providing the better prediction, by looking at the residuals between the KF frequency obtained by echo-sounding and predicted KF (Figure 9a). The prediction of

KF frequency between H_1 and H_2 is satisfactory for Au and Gl sites but not as good for He, Br and Ml sites, for which some KF frequency predictions overestimated the observations (Figure 9a).

For depths of less than H_1, the model using BPI alone is not too effective (Figure 9b). Observed frequencies varied from 10 to 64 % for all the sites, whereas predictions varied from 40 to 55 %. This indicates a limitation of the predictive model using only BPI for depths less than H_1.

In spite of these limits, the model provided good prediction of the boundary of KF disappearance H_2, on validation sites as well as on training sites (Table 4).

Predictive map

A predictive map is proposed to visualise areas where KF may occur as driven by environmental parameters (Figure 10). Three examples were taken to illustrate this map, AW, Br and Gl sites, respectively shown by black, red and blue boxes (Figure 10). <u>AW is one of the sites showing highest hydrodynamism with great V_{max} and K_{PAR} values, whereas Gl is one of the less agitated sites and Br shows an intermediate stage.</u>

KF disappear at greater depth when the water column is clear and not too cold. This is the case for the site AW site (black box, Figure 10). On this site, KF regularly reaches the 30 m depth contour. For more turbid and colder sites such as Br, KF only reaches the 20 m contour (red box, Figure 10). Exposure is also responsible for the decrease in the KF depth limit. For example, although the Gl site is clearer than AW, KF there do not reach the 30 m contour, or only very locally (blue box, Figure 10). This is explained by the lower maximum velocity at Gl than at AW (Table 1).

Simulation

In the context of Climate Change, the model was used to predict the potential variation in the KF disappearance depth, H_2, with respect to various scenarios. Simulations were based on an increase in $K_{PAR}min$ of 0.01, 0.02 and 0.05, except for locations where no turbidity data were available. For the latter, SSTmin was used with an increase of 0.2, 0.5 and 1°C. The results illustrated the antagonism of these two environmental parameters: an increase in water transparency induced an upward shift of the KF boundary while temperature was responsible for a downward one (Table 4). On sites AW, Me, Mo, Tr, Br, Gl and He (where $K_{PAR}min$ was used), H_2 decreases of 1.2 m, 1.3 m and 3.6 m were obtained with $K_{PAR}min$ respectively increasing by 0.01, 0.02 and 0.05 (Table 4). On the other hand, on sites for which SSTmin was used (Gr, Au and Ml), H_2 rose by 1, 2.5 and 5.5 m when SST respectively increased by 0.2, 0.5 and 1°C (Table 4).

DISCUSSION

Environmental effect – Antagonism between water transparency and water temperature.

Water transparency and water temperature are the two main environmental variables structuring KF frequency and distribution over the coast of Brittany. The results of this study conclude that the annual minimum value of the light attenuation coefficient by the water column is the most significant and relevant water transparency proxy for KF prediction. This minimum value is measured during spring/summer, corresponding to calm weather and thus to high water transparency because of limited sediment scouring from the bottom and river discharges. It is also during this period that maximum photosynthesis activity occurs, and the literature bears out that light attenuation by the water column is a key parameter in the structuring of macroalgae communities, essentially during spring/summer (Belsher 1986; Markager and Sand-Jensen 1992) because of this maximum photosynthesis activity. This period of the year is favourable to KF growth all the more so nutrients are not limiting factors in Brittany costal water (Ménesguen et al. 1997). This also explains why the value of the light attenuation coefficient measured during the few weeks defining the growth period is another relevant water transparency proxy for KF prediction. This is supported by calculating the percentage of incident light lightening the limit of KF disappearance. According to Markager and Send-Jensen (1992) and references within showing the percentage of incidental light ranging from 0.7 to 1.9 % reaching the depth limit for *Laminaria hyperborea,* both minimum and growth values of K_{PAR} are responsible for a percentage which is often higher than the 1% threshold permitting photosynthesis. Then, below the KF depth limit, the remaining light energy could be used by other photoautotrophic communities or organisms. KF are replaced by less dense communities, such as laminarial parks characterised by a density of less than 3 plants.m^{-2}, and shade-loving species belonging to the Rhodophyceae class like *Solieria chordalis*.

Using water transparency to predict the KF depth limit is also an interesting approach in the context of Climate Change. Climate changes, including higher temperatures, precipitation and wind speeds as well as storm events, may increase the risk of abrupt and non-linear changes in many ecosystems, which would affect their composition, function, biodiversity and productivity (IPCC 2001). Episodic events such as storms, extreme rain events and flooding resulting in strong hydrodynamics and super river discharges can lead to increased amounts of suspended mineral matter in the water column and on the bottom substrate (de Jonge and de Jong 2002; Cardoso et al. 2008). This turbidity increase is reinforced by anthropogenic activities responsible for multiple stressors including pollutants, excess nutrients, altered habitats and hydrological regimes as well as floods and droughts (Cardoso et al. 2008). The response of KF to this drop in water transparency is bound to be an upward shift of their lower limit.

Nevertheless, the KF depth limit shift due to natural or anthropogenic turbidity increases could be counterbalanced by a rise in water temperature. Indeed, this study concludes that KF take advantage of temperature increases, with communities spreading towards deeper levels. The use of water temperature for prediction is more relevant when values are measured outside of the summer period. During these warm months, water column stratification can occur and therefore surface temperature is not a good proxy for bottom temperature. The rest of the year, when the water column is fairly homogenous and the bottom water is slightly cooler than at the surface, surface temperature is a good proxy for the entire column. Next, one of the structuring factors of Brittany KF communities is a minimum value of surface temperature measured during winter, varying from 8.3 to 9.6 ℃. These low temperatures are without consequences for *Laminaria digitata*, the major species providing high KF levels (approximately from the LAT down to a depth of 5 m), as their broad ecological optimum varies from 3 to 15 ℃ (Belsher 1986). On the other hand, *L. hyperborea*, the major species making up the lower-lying part of KF (approximately from LAT to the depth limit) is more sensitive to cold temperature. Its optimum is narrower than that of *L. digitata*, varying from 10 to 17 ℃ and young sporophyte growth is altered at temperatures less than 10 ℃ (Belsher 1986). This explains why a rise in colder temperatures favours the spreading of these communities towards deeper levels. Using temperature measured during the cold period for predictions is also an interesting approach in the case of Climate Change, because water warming is mainly observed during this period (Koutsikopoulos et al. 1998). Nevertheless, although an increase in the coldest temperatures, as a consequence of Climate Change, seems to favour a downward KF shift, this phenomenon could be moderated or even reversed by the decrease in water transparency during calm periods. These two parameters have an antagonistic effect on KF structure.

Moreover, although the current model was not able to predict an effect on KF upper limits, the temperature increase observed over the past decades (IPCC 2001) could have an harmful effect on them. Indeed, *L. digitata* which occupies the upper part of KF, shows an optimum until 15℃, and a lethal temperature value around 23 - 24 ℃ (Belsher 1986). The latter values have not been observed along the coast of Brittany using the AVHRR scale, but, if surface temperatures kept increasing (as could be the case locally), lethal values would soon be reached. This warming effect would lead to KF reaching deeper and cooler water.

Then, in the worse Climate Change scenario, showing a rapid, high rise in temperature with an increase in the number and intensity of extreme events (IPCC, 2001), the consequences will be an upward shift of the depth limit and a downward one of the upper KF boundary, leading to a reduction in their width. If worse comes to worst, the effects of both an increase in water temperature and a decrease in transparency could lead to the complete disappearance of KF. This dramatic consequence would lower or eliminate the habitat surface area and alter the diversity, abundance and functioning of the associated biological communities. This depletion of the ecosystem will also have economic consequences because of the decrease of this resource already threatened by over-cropping (MEDD 2005). All these consequences will be irremediable if no global resolution like that recommended by the Intergovernmental Panel on Climate Change (IPCC, http://www.ipcc.ch) is adopted in the next few years.

Environment effect – Bed stress issue

Although the main studies assessing macro-algae with regard to exposure involve wave swell effects and the intertidal area (Denny 1995; Hurd 2000; Denny and Gaylord 2002; Buck and Buchholz 2005; Boller and Carrington 2006), this study considered exposure due to tidal currents. Numerous authors have shown the effect of orbital wave velocity, responsible for a drag force tending to push an object downstream, which depends on the water density and velocity exponent of drag, β (Denny 1995). This exponent is derived from Vogel's *E* (Vogel 1994), and measures the relationship between velocity and drag. It determines how force increases with an increase in water velocity. For bluff objects subjected to drag, β is approximately 2 (Denny 1995; Denny and Gaylord 2002) and numerous authors take this value for all objects, whether flexible or not (Buck and Buchholz 2005; Boller and Carrington 2006; Pope et al. 2006). However, Vogel (1994) and Denny (1995) suggest that an exponent value lesser than 2 be used for streamlined or flexible objects. Indeed, in a unidirectional flow, algal fronds bend in response to the force applied, and the plant reorients and rearranges itself passively in a way resulting in overall streamlining (Denny 1995 and references within). Consequently, the β for exposed algae in flow is universally less than 2 and typically around 1.5 (Denny 1995), with the velocity-dependant character of shape being incorporated in this exponent. In this study, because of the lack of swell data for the entire survey area at an appropriate scale, the effect of tidal current velocity was tested as a proxy for global water motion. The results confirm Denny's suggestion: the value 1.5 for velocity exponent of drag is more significant than the value 2, although water velocity does not have the same source (swell *vs.* tide). The effect of a velocity increase is positive for KF: for sites with the same water transparency conditions, a velocity greater than 0.8 $m.s^{-1}$ induces a downward shift of KF depth limit. This could be explained by a regular cleaning effect of thalli in wild sites, making them more receptive to photosynthetically available radiation than in sheltered sites where thalli are often covered with a thin layer of particles. On the other hand, and although this has not been observed on the scale and the sites of this study, too high a velocity is not beneficial for KF, which could be dislodged or destroyed, as shown *in situ* or experimentally for a number of macroalgae species (Gaylord et al. 2003; Buck and Buchholz 2005; Boller and Carrington 2006). Indeed, the shear stress imposed on a structure by water velocity of 2 $m.s^{-1}$ is roughly equivalent to that exerted by wind of 130 $mils.h^{-1}$ (Denny and Gaylord 2002).

Another proxy for exposure is the topography. This environmental variable is the only one explaining KF structures when water temperature and transparency are not limiting factors, that is to say in shallow depths. KF are observed more often, on a working scale, in depressions rather than on crests. This could be explained by the fact that crests are too exposed to the swell and tidal currents and therefore KF would be overly subjected to high drag forces. These forces are lower in depressions where KF are more sheltered. This explanation must be advanced with caution, because the expected result involving the topography was a greater occurrence of KF on crests rather than depressions (S. Derrien, *com.pers.*). Indeed, global topography as used in this study is not efficient enough to predict KF variability correctly in shallow water which leads to limited prediction between LAT and H_1. The BPI computed on a finer scale than the one used here at a 150m resolution, was expected to be a more reliable variable to explain KF distribution at shallower depths. The availability of proper high resolution depth data over the entire extent of the coast of Brittany remains a major issue. This leads us to data quality issues.

Data quality – limitations and scale problem

The digital echo sounding system successfully characterised KF in the surveyed areas and again demonstrated its ability to characterise and map aquatic vegetation, as shown and validated in previous studies (McRea et al. 1999; Piazzi et al. 2000; Brown et al. 2002; Freitas et al. 2003; Riegl et al. 2005; Freitas et al. 2006). Nevertheless, the acoustic detection showed some limitations. The first one is the binary classification of substratum: rock or not. Since the survey was conducted with quite a small vessel, the results are sensitive to weather conditions and it is recommended that surveys be conducted under calm weather conditions (without swell and wind). Typical problems include: false KF detection, inaccuracy in the evaluation of the instantaneous depth and number of *Bottom Errors* increasing with wave height, leading to a degraded acoustic dataset. Research is still under way and better results are expected with the improvement of the clustering algorithm, particularly on some critical points:

- A decrease in the number of *Bottom Errors*. This would reduce the number of misdetection of KF, especially on rocky substrata.
- A better submerged aquatic vegetation classification. For this study, transects were mainly assessed in pure KF areas, but in some locations (particularly in very shallow waters), different submerged aquatic vegetation species could be

present (*Zostera marina* on the AW site, for example) and influence the classifying procedure. Better knowledge of the different species spectral signatures and taking them into account in the algorithm would reduce KF false detection.

Another type of input data required with the highest possible quality is the substratum layer. KF are predicted only where a rocky substrate is present, by way of a mask of the rocky area. At the working scale, i.e., pixels of 150 m covering the entire coast of Brittany, these prediction errors are without consequences, since the obtained map provides the prediction of the distribution and the inter-site variation of KF frequencies at a global scale. However, if this model was adapted to finer scales in order to predict local distributions and intra-site variations of KF, the current scale of the substratum layer (not better than 1:500,000) would not be efficient and would have to be refined. High resolution Lidar data, for example, could overcome this limitation at a local scale. The ability of Lidar data to finely characterise seabed substratum types was tested in recent studies (Rosso et al. 2006; Méléder et al. 2007). Its high vertical and horizontal accuracy make it suitable to map bottom roughness and topography in great detail (although at a high cost!).

Obviously, a good balance should be sought in scale homogeneity between source data. For example, distribution laws as a function of depth used for model calibration and validation were established using field bathymetry data from echo soundings, whereas the model input raster dataset used for prediction was generated from various sources at various resolutions (a mix of Lidar, digital soundings and map soundings). Depth values from these two sources (map *vs.* field) exhibit discrepancies leading to misprediction. For example, KF could be predicted on the map for an area where field depths were too great to be photosynthetically efficient or conversely, some map areas where no KF were predicted corresponded to small field depths allowing KF growth.

At the end of day, satellite data from SeaWiFS and AVHRR used are in accordance with the current working scale for prediction at regional scale. However, similarly to the substratum and bathymetry issues, image resolution limits the use of the model for prediction at a local scale. MERIS, an ocean colour sensor aboard the Envisat satellite, with a pixel resolution of 300 m, will also allow progress towards finer scales.

While progress is expected from regional to local levels, additional parameters may have to be introduced in the model, as they may have an effect on KF at local scale, and this would require new investigations. For example, the effect of faunal abundance consuming primary producers or the swell effect through drag forces and/or abrasion of rocky area by sand, fine topography, must be tested.

CONCLUSION

The proposed model enabled the prediction of KF frequency over time and space as a function of water transparency and exposure, at a global scale that is effective in the context of Climate Change. Its main limits were: a) predictions in shallow water where the bathymetry at the working scale was not fine enough and b) the mostly coarse scale of source data which did not allow local effects to be assessed. These two limits could be overcome with an adaptation of the model, including refinement of the working source data and the addition of new key parameters influencing communities at local scales. Nevertheless, the current model is a good decisional tool at a global scale, as in the context of Climate Change, allowing us to predict changes in the KF depth limit which could be used as an indicator of the health of these communities and those associated with them.

REFERENCES

Bajjouk T, Guillaumont B, Populus J (1996) Application of airborne imaging spectrometry system data to intertidal seaweed classification and mapping. HYDROBIOLOGIA 327: 463-471

Belsher T (1986) Etude bibliographique de quelques espèces planctoniques et benthiques de la Manche. Vol. 4 : Phytobenthos. Ifremer, Brest

Boller ML, Carrington E (2006) The hydrodynamic effects of shape and size change during reconfiguration of a flexible macroalga. J EXP BIOL 209: 1894-1903

Brinkman AG, Dankers N, van Stralen M (2002) An analysis of mussel bed habitats in the Dutch Wadden Sea. HELGOLAND MAR RES 56: 59-75

Brown CJ, Cooper KM, Meadows WJ, Limpenny DS, Rees HL (2002) Small-scale mapping of sea-bed assemblages in the eastern English Channel using sidescan sonar and remote sampling techniques. ESTUAR COAST SHELF S 54: 263-278

Buck BH, Buchholz CM (2005) Response of offshore cultivated *Laminaria saccharina* to hydrodynamic forcing in the North Sea. AQUACULTURE 250: 674-691

Cardoso PG, Raffaelli D, Lillebø AI, Verdelhos T, Pardal MA (2008) The impact of extreme flodding events and anthropogenic stressors on macrobenthic communities' dynamics. ESTUAR COAST SHELF S 76: 553-565

Combe JP, Launeau P, Carrere V, Despan D, Meleder V, Barille L, Sotin C (2005) Mapping microphytobenthos biomass by non-linear inversion of visible-infrared hyperspectral images. REMOTE SENS ENVIRON 98: 371-387

Dayton PK, Tegner MJ, Parnell PE, Edwards PB (1992) Temporal and spatial patterns of disturbance and recovery in a kelp forest community. ECOL MONOGR 62: 421-445

de Jonge VN, de Jong DJ (2002) 'Global Change' impact of inter-annual variation in water discharge as a driving factor of dredging and spoil disposal in the river Rhine system and of turbidity in the Wadden sea. ESTUAR COAST SHELF S 55: 969-991

De Oliveira E, Populus J, Guillaumont B (2006) Predictive modelling of coastal habitats using remote sensing data and fuzzy logic. EARSeL eProceedings 5: 208-223

Denny M (1995) Predicting physical disturbance: mechanistic approaches to the study of survivorship on wave-swept shores. ECOL MONOGR 65: 371-418

Denny M, Gaylord B (2002) The mechanics of wave-swept algae. J EXP BIOL 205: 1355-1362

Ferrat L, Pergent-Martini C, Roméo M (2003) Assessment of the use of biomarkers in aquatic plants for the evaluation of environmental quality: application to seagrasses. AQUAT TOXICOL 65: 187-204

Freitas R, Rodrigues AM, Quintino V (2003) Benthic biotopes remote sensing using acoustics. J EXP MAR BIOL ECOL 285-286: 339-353

Freitas R, Sampaio L, J. O, Rodrigues AM, Quintino V (2006) Validation of soft bottom benthic habitats identified by single-beam acoustics. MAR POLLUT BULL 53: 72-79

Gaylord B, Denny M, Koehl MAR (2003) Modulation of wave forces on kelp canopies by alongshore currents. LIMNOL OCEANOGR 48: 860-871

Gohin F, Loyer S, Lunven M, Labry C, Froidefond J-M, Delmas D, Huret M, Herbland A (2005) Satellite-derived parameters for biological modelling in coastal waters: Illustration over the eastern continental shelf of the Bay of Biscay. REMOTE SENS ENVIRON 95: 29-46

Greve TM, Krause-Jensen D (2005) Predictive modelling of eelgrass (Zostera marina) depth limits. MAR BIOL 146: 849-858

Guillaumont B, Bajjouk T, Talec P (1997) Seaweed and remote sensing: a critical review of sensors and data processing. In: Round FE, Chapman DJ (eds) Progress in Phycological Research. Biopress, pp 213-282

Guillaumont B, Callens L, Dion P (1993) Spatial-Distribution and Quantification of Fucus Species and Ascophyllum-Nodosum Beds in Intertidal Zones Using Spot Imagery. HYDROBIOLOGIA 261: 297-305

Hurd CL (2000) Water motion, marine macroalgae, physiology, and production. J PHYCOL 36: 453-472

IPCC (2001) Climate change 2001: the scientific basis, contribution of working group I to the third assessment report of the Intergovernmental Panel on Climate Change (IPCC). Cambridge University Press, Cambridge

Kelly NM, Fonseca M, Whitfield P (2001) Predictive mapping for management and conservation of seagrass beds in North Carolina. AQUAT CONSERV 11: 437-451

Koutsikopoulos C, Beillois P, Leroy C, Taillefer F (1998) Temporal trends ans spatial structures of the sea surface temperature in the Bay of Biscay. OCEANOL ACTA 21: 335-344

Lundblad ER, Wright DJ, Naar DF, Donahue BT, Miller J, Larkin EM, Rinehart R (2004) Classifying deep water benthic habitats around Tutulia, America Samoa 24th annual ESRI Conference, San Diego, CA

Marchalot C, Diner N, Berger L (2003) MOVIES+ documentation: Echo-integration by depth layers using MOVIES+ software. IFREMER/DNIS/ESI, Plouzané

Markager S, Sand-Jensen K (1992) Light requirements and depth zonation of marine macroalgae. MAR ECOL-PROG SER 88: 83-92

McRea JE, Greene HG, O'Connell VM, Wakefield WW (1999) Mapping marine habitats with high resolution sidescan sonar. OCEANOL ACTA 22: 679-686

MEDD (2005) Plan d'actions stratégique du MEDD pour les milieux marins. Tome 1 - Diagnostic et Orientations. Ministère de l'écologie et du développement durable, Paris

Méléder V, Launeau P, Barillé L, Rincé Y (2003) Microphytobenthos assemblage mapping by spatial visible-infrared remote sensing in a shellfish ecosystem. C R BIOL 11: 437-451

Méléder V, Populus J, Rollet C (2007) Mapping seabed substrata using Lidar remote sensing. MESH - Mapping European Seabed Habitats. http://www.searchmesh.net/PDF/GMHM3_Mapping_Substrata_using_LIDAR.pdf

Ménesguen A, Piriou JY, Dion P, Auby I (1997) Les "Marées vertes", un exemple d'eutrophisation à macroalgues. In: Dauvin J-C (ed) Les biocénoses marines et littorales françaises des côtes atlantiques, Manche et Mer du Nord. Synhtèse, menaces et perspectives. MNHN, Paris, pp 212-218

Norderhaug KM, Christie H, Rinde E (2002) Colonisation of kelp imitations by epiphyte and holdfast fauna; a study of mobility patterns. MAR BIOL 141: 965-973

Piazzi L, Acunto S, Cinelli F (2000) Mapping of *Posidonia oceanica* beds around Elba Island (western Mediterranean) with integration of direct and indirect methods. OCEANOL ACTA 23: 339-346

Pope ND, Widdows J, Brinsley MD (2006) Estimation of bed shear stress using the turbulent kinetic energy approach. A comparison of annular flume and field data. CONT SHELF RES 26: 959-970
Riegl BM, Moyer RP, Morris LJ, Virnstein RW, Purkis SJ (2005) Distribution and seasonal biomass of drift macroalgae in the Indian River Lagoon (Florida, USA) estimated with acoustic seafloor classification (QTCView, Echo*plus*). J EXP MAR BIOL ECOL 326: 89-104
Roff JC, Taylor ME (2000) National frameworks for marine conservation - A hierarchical geophysical approach. AQUAT CONSERV 10: 209-223
Rosso PH, Ustin SL, Hastings A (2006) Use of lidar changes associated with *Spartina* invasion in San Francisco Bay marshes. REMOTE SENS ENVIRON 100: 295-306
SHOM (1994-2005) Cartes sédimentologiques (G). SHOM
Sivertsen K (1997) Geographic and environmental factors affecting the distribution of kelp beds and barren grounds and changes in biota associated with kelp reduction at sites along the Norwegian coast. CAN J FISH AQUAT SCI 54: 2872-2887
Stevens T, Connolly RM (2004) Testing the utility of abiotic surrogates for marine habitat mapping at scales relevant to management. BIOL CONSERV 119: 351-362
Toms JD, Lesperance ML (2003) Piecewise regression: A tool for identifying ecological thresholds. ECOLOGY 84: 2034-2041
Vaslet D, Larsonneur C, Auffret J-P (1979) Carte des sédiments superficiels de la Manche. BRGM/CNEXO
Vogel S (1994) Life in Moving Fluids (2nd edn). Princeton University Press, Princeton, pp 467 pp.
Zacharias MA, Morris MC, Howes DE (1999) Large scale characterization of intertidal communities using a predictive model. J EXP MAR BIOL ECOL 239: 223-242
Zacharias MA, Roff JC (2001) Explanations of patterns of intertidal diversity at regional scales. J BIOGEOGR 28: 471-483

Figure legend

Figure 1. Location of the 10 sites. Black star: sites used to build the model; white star: sites used to validate it.

Figure 2. Echo-integration by depth layers in dense kelp forest (KF) on a selected part of the acoustic transect. A: bottom line – Seafloor; B: offset line – down limit of the Kelp forest integrated layer (0.2 meters above bottom); C: Top limit of the integrated layer (2.2 meters above bottom). The vertical lines delimit each ESU (20 ping width).

Figure 3. Kelp forest frequency *vs.* depth. Example from the site Molène, Mo (cf. Figure 1). Observations (O) are obtained from echo-sounding and are fitted using piecewise regression (bold line), fixing the two breakpoints, H_1 and H_2, and the slope between these points, $Slope_2$. Fit is expressed with its prediction (fine line) and confidence (dashed line) intervals at 95 %.

Figure 4. Weekly water transparency, expressed in K_{PAR}, derived from SeaWiFS data averaged over the 1998-2004 period. a/ Sites used for model building; b/ Sites used for model validation.

Figure 5. Weekly temperature, expressed in SST, derived from AVHRR data averaged over the two past decades. a/ Sites used for model building; b/ Sites used for model validation.

Figure 6. Example of an echogram along a selected acoustic transect (from Gl site, cf. Figure 1). The results of the cluster analysis classification procedure of KF presence (LAMINAIRE) or absence (empty box) are presented in table above echogram with the corresponding bathymetry (m). For *BOTT-ERR* definition, see Materials and Methods section.

Figure 7. KF frequency observed *vs.* predicted with the four significant models for depth ranging from H_1 to H_2 at the five sites used to build model: AW, Mo, Me, Tr and Gr. a/ pred_mod1: model using SSTmin only (eqs. 11 to 13), b/ pred_mod2: model using K_{PAR}min (eqs. 14 to 16), c/ pred_mod3: model using K_{PAR}min and $Vmax^{1.5}$ (eqs. 14, 16 and 17), d/ pred_mod4: model using SSTmin and $Vmax^{1.5}$ (eqs. 11, 13 and 18). Dark lines illustrate the relationship observation = prediction.

Figure 8. KF frequency observed *vs.* predicted using BPI (eq. 9), for depth less than H_1 at the five sites used to build model: AW, Mo, Me, Tr and Gr. Dark lines illustrate the relationship observation = prediction.

Figure 9. Model validation. KF frequency observed *vs.* predicted at the five sites used to valid model: Au, Br, Gl, He, Ml. a/ prediction for depth ranging from H_1 to H_2 using K_{PAR}min and $Vmax^{1.5}$ (pred_mod3; eqs. 14, 16 and 17), or SSTmin and $Vmax^{1.5}$ (pred_mod4; eqs. 11, 13 and 18) when no turbidity data are available; b/ prediction for depth less than H_1 using BPI (eq. 19).

Figure 10. Predictive map of KF presence percentage. Three zooms are shown to illustrate results: AW, Br and Gl, respectively in black, red and blue boxes.

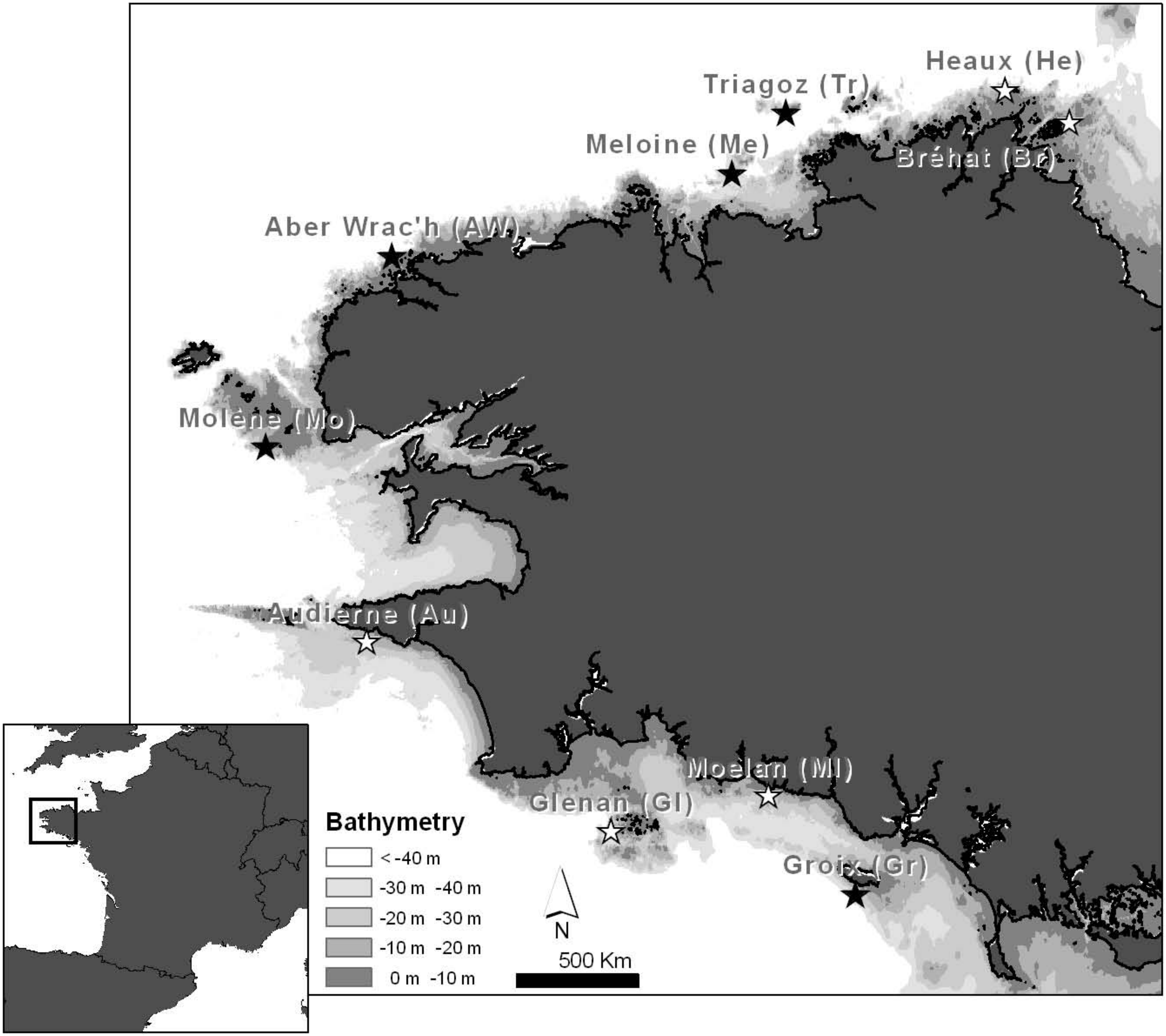

Heaux (He)
Triagoz (Tr)
Meloine (Me)
Bréhat (Br)
Aber Wrac'h (AW)
Molène (Mo)
Audierne (Au)
Moëlan (Ml)
Glenan (Gl)
Groix (Gr)
Bathymetry
< -40 m
-30 m -40 m
-20 m -30 m
-10 m -20 m
0 m -10 m
N
500 Km

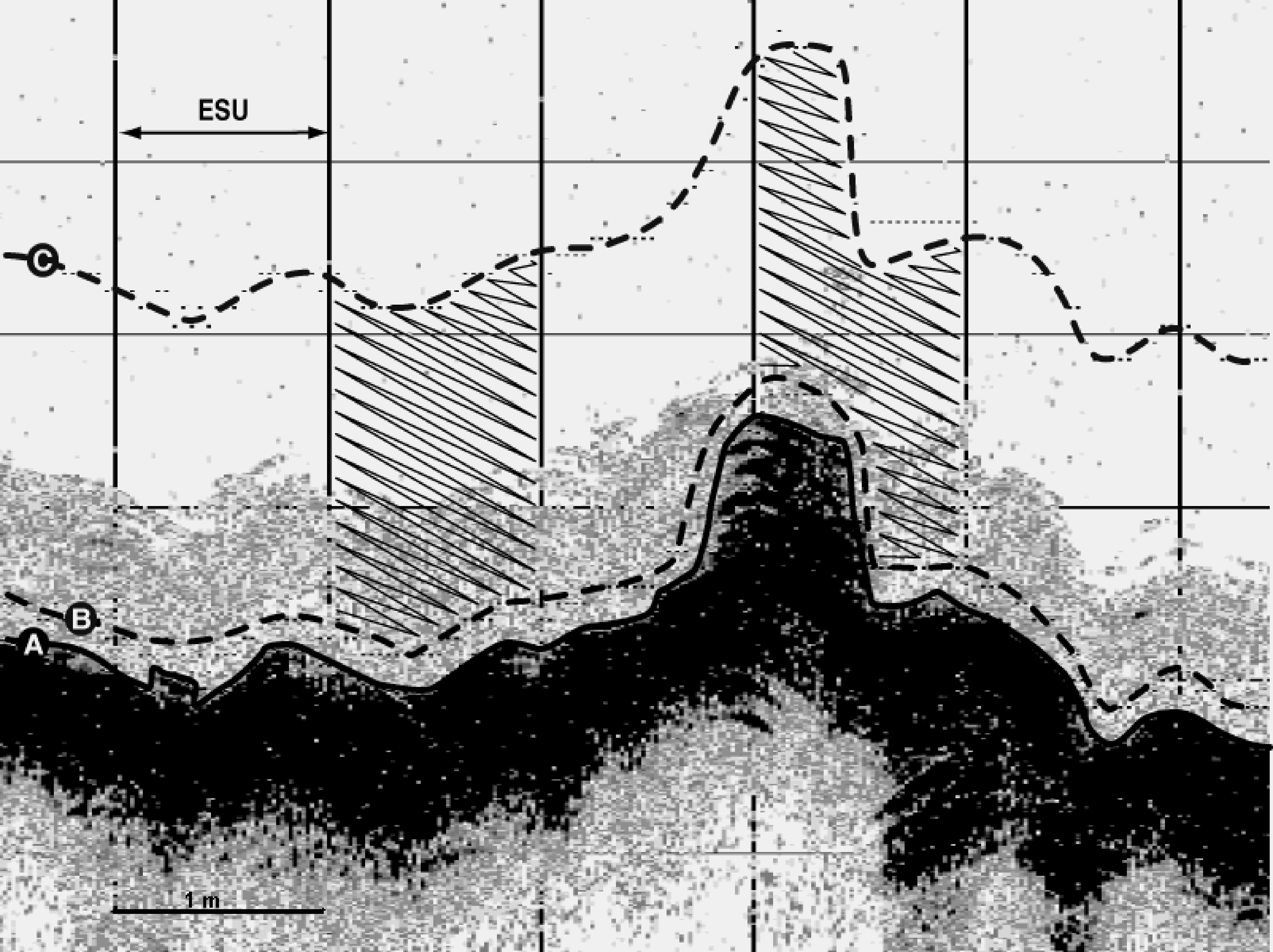

ESU
C
B
A
1 m

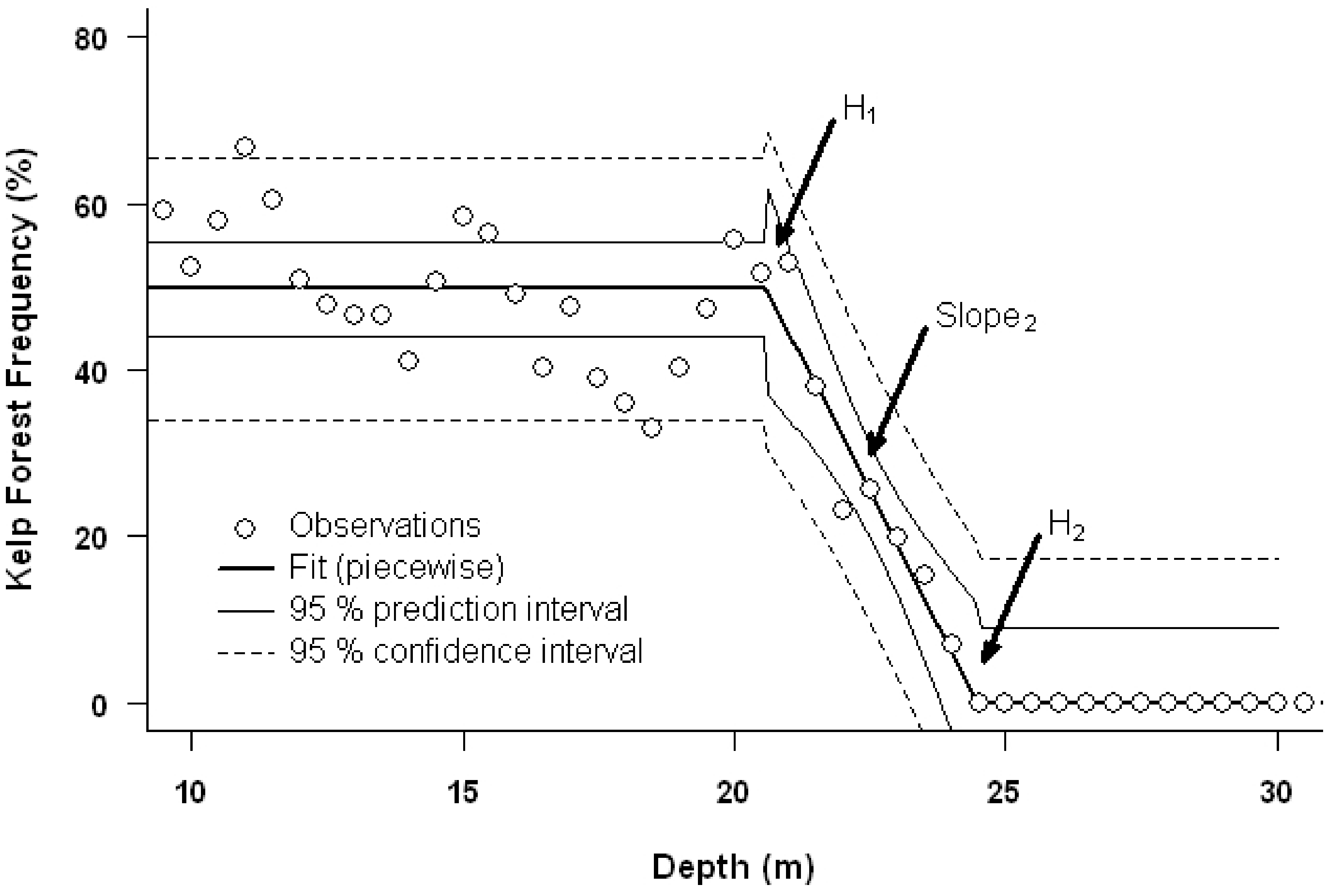

80
60
40
20
0
Kelp Forest Frequency (%)
10
15
20
25
30
Depth (m)
H1
Slope 2
H2
Observations
Fit (piecewise)
95 % prediction interval
95 % confidence interval

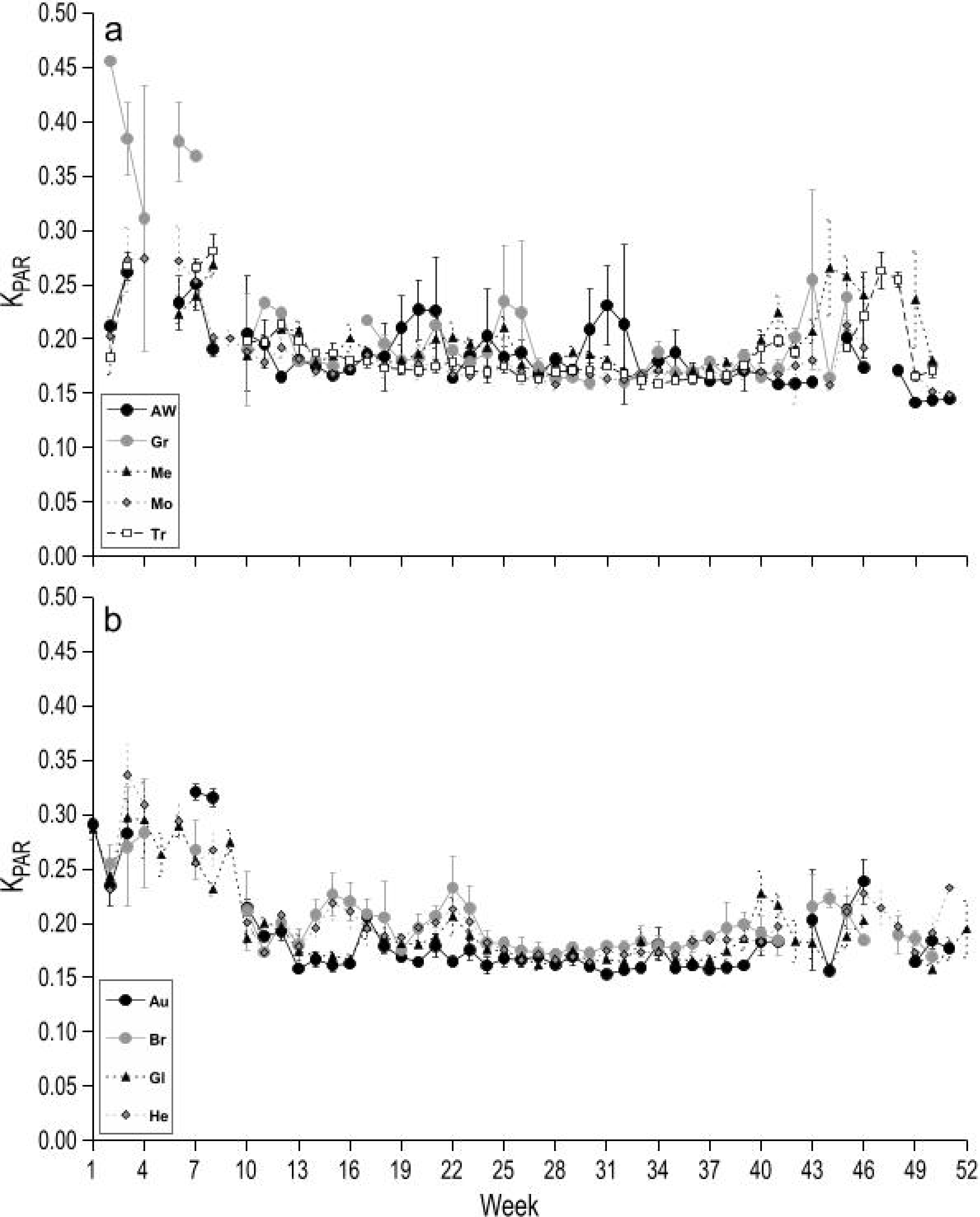

a
b
KPAR
Week
AW
Gr
Me
Mo
Tr
Au
Br
Gl
He
0.00
0.05
0.10
0.15
0.20
0.25
0.30
0.35
0.40
0.45
0.50
1
4
7
10
13
16
19
22
25
28
31
34
37
40
43
46
49
52

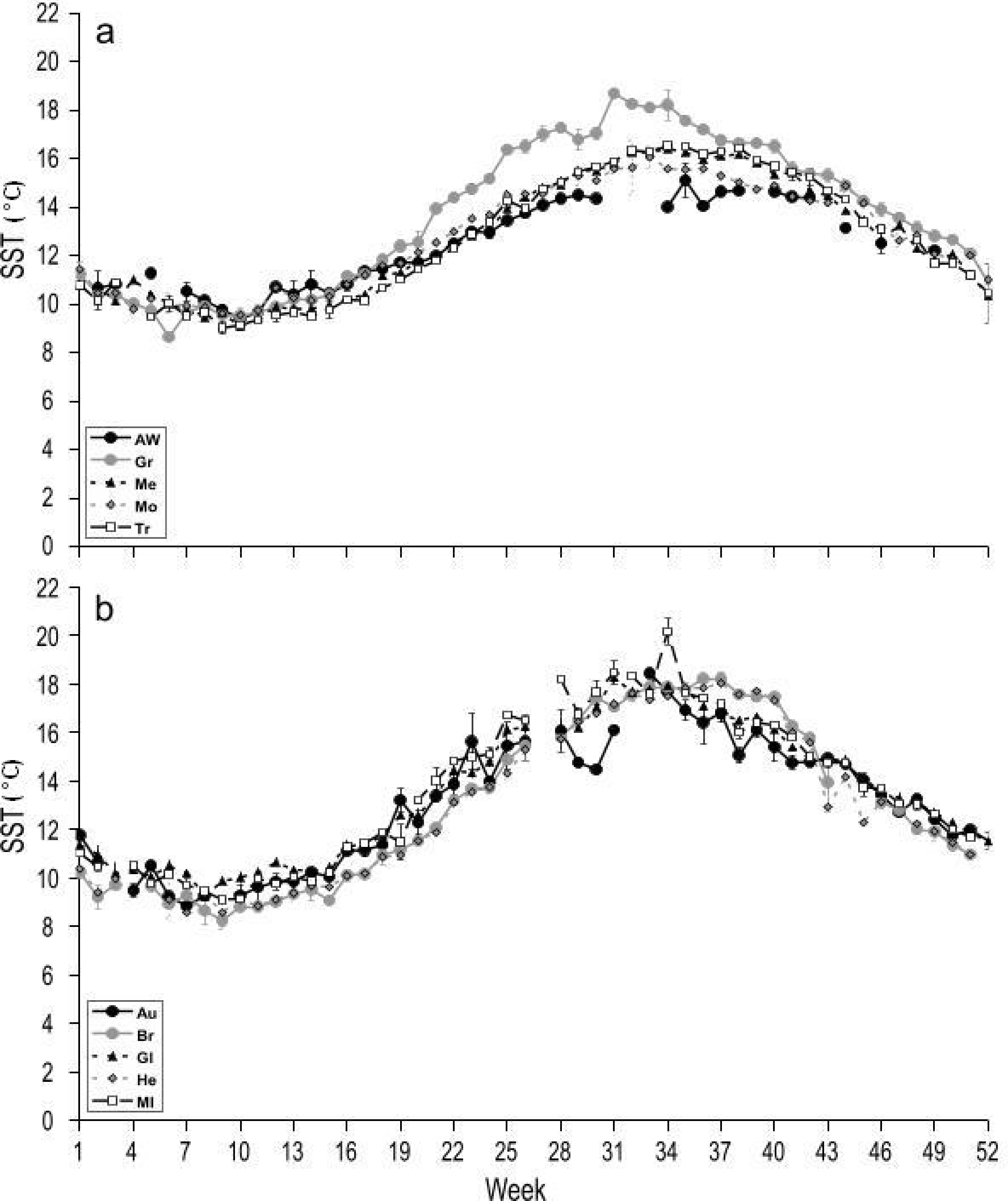

a
b
SST (°C)
Week
AW
Gr
Me
Mo
Tr
Au
Br
Gl
He
Ml

TPS	Z_corr	Classif 2
12:58:48	9,63	LAMINAIRE
12:58:49	10,13	LAMINAIRE
12:58:50	10,03	
12:58:51	10,33	BOTT-ERR
12:58:52	10,33	
12:58:52	10,23	BOTT-ERR
12:58:53	10,13	BOTT-ERR
12:58:54	9,53	BOTT-ERR
12:58:55	9,63	LAMINAIRE
12:58:56	10,23	LAMINAIRE
12:58:56	10,53	LAMINAIRE
12:58:57	10,83	LAMINAIRE
12:58:58	11,03	LAMINAIRE
12:58:59	11,23	LAMINAIRE
12:59:00	11,03	
12:59:01	11,13	LAMINAIRE
12:59:01	11,63	
12:59:02	11,33	BOTT-ERR
12:59:03	12,03	BOTT-ERR
12:59:04	11,33	BOTT-ERR
12:59:05	11,73	
12:59:06	12,43	BOTT-ERR
12:59:07	12,23	LAMINAIRE
12:59:08	12,33	LAMINAIRE
12:59:08	12,73	
12:59:09	12,93	
12:59:10	13,24	BOTT-ERR
12:59:11	12,74	LAMINAIRE
12:59:12	12,84	
12:59:13	13,14	
12:59:14	13,04	
12:59:15	12,94	
12:59:16	12,34	LAMINAIRE
12:59:17	12,54	LAMINAIRE
12:59:18	12,24	LAMINAIRE
12:59:19	12,74	BOTT-ERR
12:59:20	12,34	
12:59:21	13,04	LAMINAIRE
12:59:21	12,94	LAMINAIRE
12:59:22	12,84	LAMINAIRE
12:59:23	13,14	LAMINAIRE
12:59:24	13,04	
12:59:25	12,84	LAMINAIRE
12:59:26	12,84	LAMINAIRE
12:59:27	12,94	LAMINAIRE
12:59:28	12,44	LAMINAIRE
12:59:29	12,54	LAMINAIRE
12:59:30	12,64	LAMINAIRE
12:59:31	11,94	LAMINAIRE
12:59:32	11,64	LAMINAIRE
12:59:33	11,34	LAMINAIRE

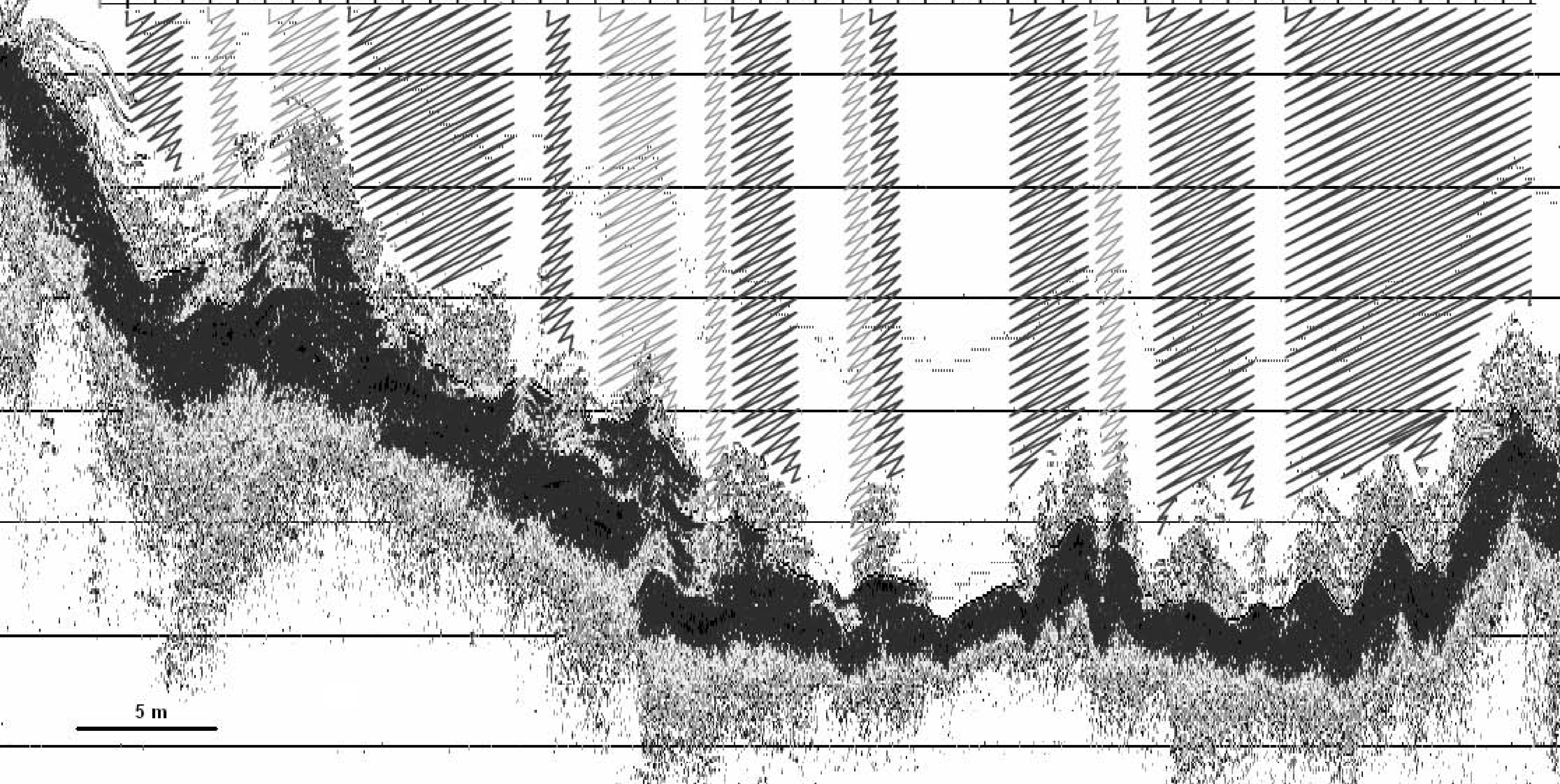

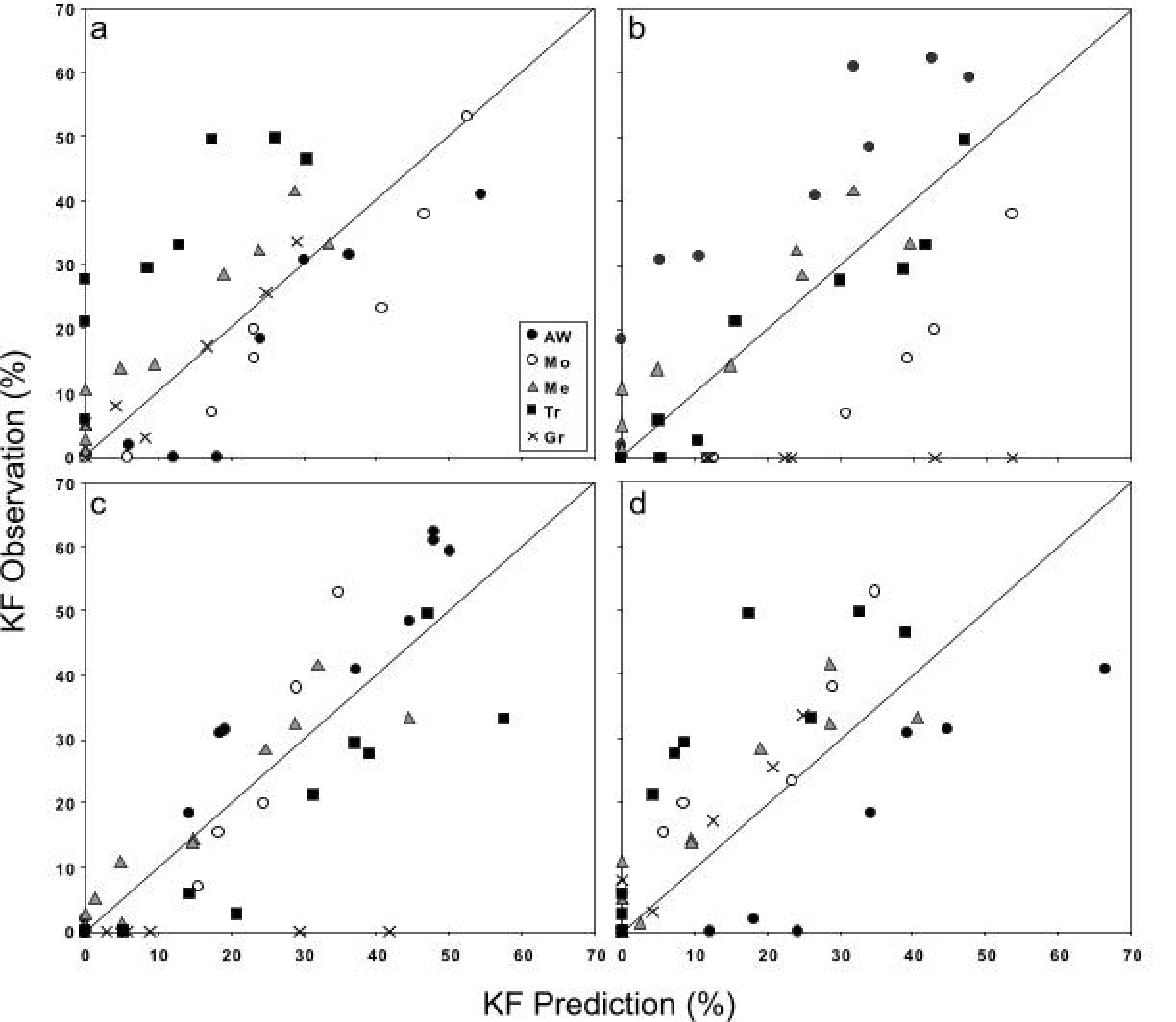

a
b
c
d
AW
Mo
Me
Tr
Gr
KF Observation (%)
KF Prediction (%)
0
10
20
30
40
50
60
70

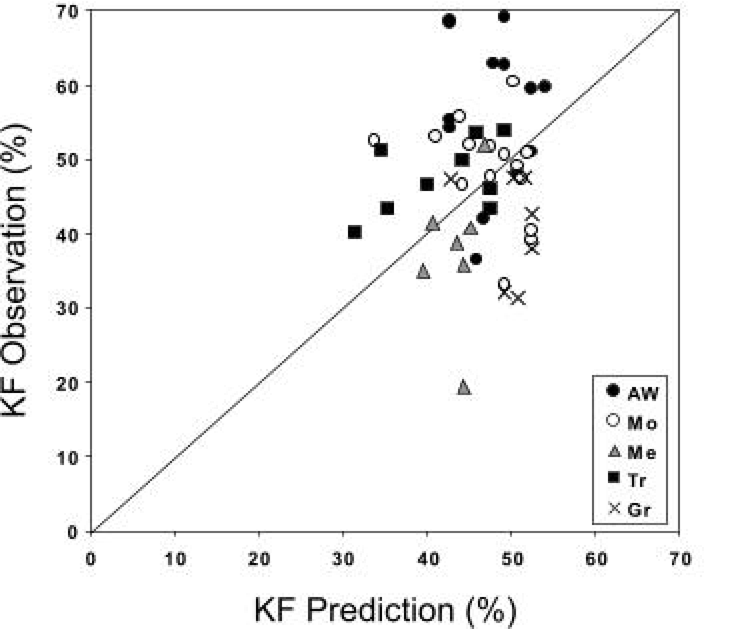
KF Observation (%)
KF Prediction (%)
0
10
20
30
40
50
60
70
AW
Mo
Me
Tr
Gr

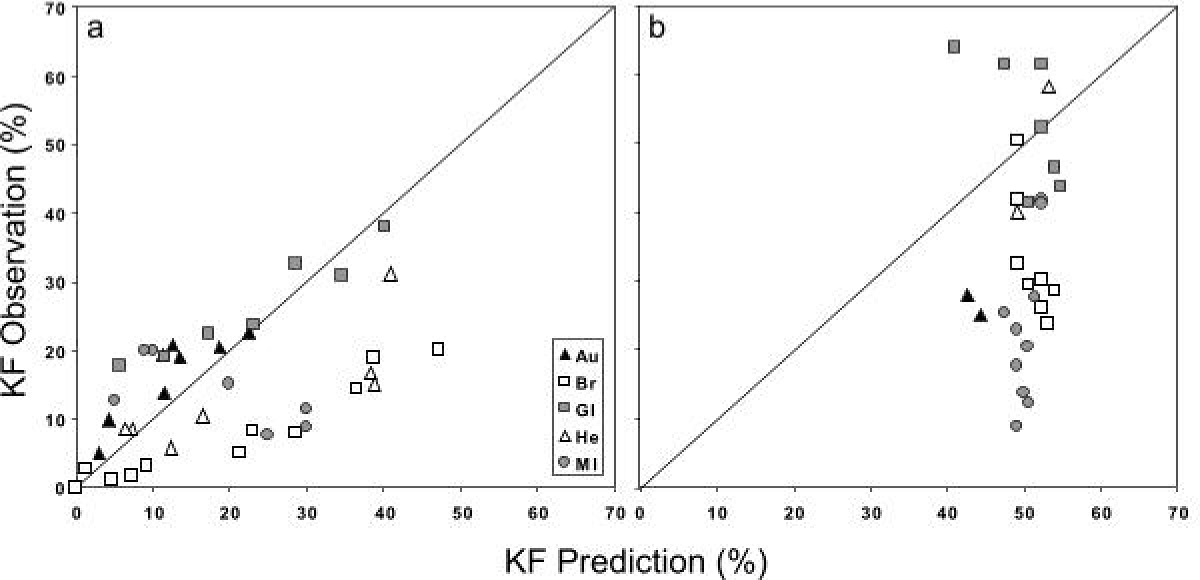

a
b
Au
Br
Gl
He
Ml
KF Observation (%)
KF Prediction (%)
0
10
20
30
40
50
60
70

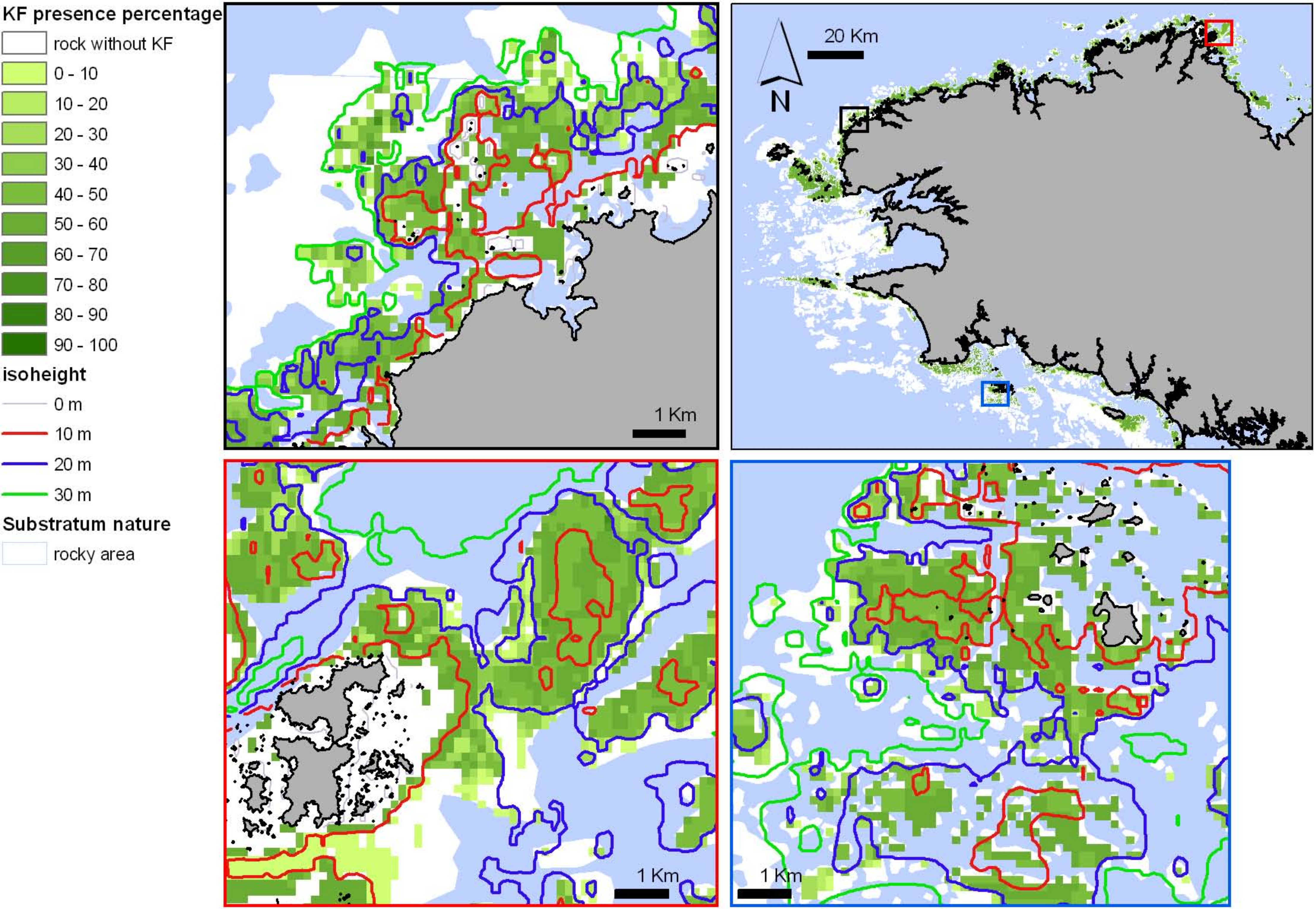

KF presence percentage
rock without KF
0 - 10
10 - 20
20 - 30
30 - 40
40 - 50
50 - 60
60 - 70
70 - 80
80 - 90
90 - 100
isoheight
0 m
10 m
20 m
30 m
Substratum nature
rocky area
1 Km
20 Km
N
1 Km
1 Km

Table 1. Environmental parameters used in stepwise regression processes. Training sites are underlined, the others are validation sites.

	K_{PAR}year	K_{PAR}growth	K_{PAR}min	K_{PAR}max	SSTyear	SSTgrowth	SSTmin	SSTmax	Vmax
AW	0.201	0.190	0.175	0.261	12.4	11.9	9.4	15.1	1.12
Gr	0.265	0.194	0.202	0.456	13.6	12.9	8.7	18.7	0.27
Me	0.215	0.191	0.183	0.268	12.7	11.6	9.1	16.4	0.89
Mo	0.197	0.173	0.160	0.274	12.8	12.1	9.6	16.1	0.27
Tr	0.202	0.176	0.176	0.281	12.7	11.5	9.0	16.5	0.95
Au	0.205	0.171	0.164	0.321	13.1	12.7	8.9	18.5	0.44
Br	0.220	0.205	0.189	0.283	13.0	11.7	8.3	18.2	0.87
Gl	0.218	0.182	0.164	0.297	13.5	12.8	9.3	18.3	0.27
He	0.222	0.197	0.182	0.337	13.0	11.6	8.6	18.0	0.87
Ml	-	-	-	-	13.7	12.9	9.1	20.2	0.1

Table 2. Breakpoints H_1 and H_2 and the slope between them, $Slope_2$, fitted using piecewise regressions. All regressions and fit parameters are significant ($p \leq 0.01$) except for sites Au, He and Ml (n.s: not significant). Training sites are underlined, the others are validation sites.

	<u>AW</u>	<u>Gr</u>	<u>Me</u>	<u>Mo</u>	<u>Tr</u>	Au	Br	Gl	He	Ml
adjusted R^2	0.92	0.96	0.88	0.90	0.96	0.80	0.92	0.98	0.98	0.97
$H_1 \pm$ std	19.9 ± 0.4	15.5 ± 0.4	19.3 ± 0.6	20.6 ± 0.5	18.8 ± 0.4	n.s.	13.2 ± 0.6	15.2 ± 0.3	15.5 ± 0.1	n.s.
$Slope_2 \pm$ std	-11.5 ± 1.5	-8.9 ± 0.8	-8.8 ± 0.9	-12.5 ± 0.8	-9.3 ± 1.1	-3.6 ± 0.4	-4.9 ± 0.4	-6.0 ± 0.2	n.s.	n.s.
$H_2 \pm$ std	25.2 ± 0.5	19.6 ± 0.4	23.4 ± 0.6	24.5 ± 0.6	23.8 ± 0.4	22.3 ± 1.6	21.7 ± 0.8	25.8 ± 0.4	27.8 ± 1.4	22.3 ± 0.8

Table 3. Fraction of incident light (in %), Fr, reaching KF depth limit H_2. Fr values are calculated (eq. 1) for four water transparency variables: K_{PAR}year, K_{PAR}growth, K_{PAR}min and K_{PAR}max. Fr is not estimated for the site Ml, because no turbidity data are available. Training sites are underlined, the others are validation sites.

	Fr_{H_2} (K_{PAR}year)	Fr_{H_2} (K_{PAR}growth)	Fr_{H_2} (K_{PAR}min)	Fr_{H_2} (K_{PAR}max)
<u>AW</u>	0.66	0.80	1.26	0.15
<u>Gr</u>	0.57	2.32	1.95	0.62
<u>Me</u>	0.64	1.17	1.36	0.18
<u>Mo</u>	0.80	1.41	1.98	0.12
<u>Tr</u>	0.78	1.51	1.46	0.12
Au	1.04	2.19	2.56	0.08
Br	0.84	1.17	1.65	0.21
Gl	0.36	0.91	1.44	0.05
He	0.21	0.42	0.63	0.01
Ml	-	-	-	-

Table 4. Prediction of KF depth limit H_2. Observed H_2 are from piecewise regression (Table 2), predicted and simulated H_2 are from predictive model (pred_mod3 or pred_mod4*) but simulated ones follow varied scenarios (see text for detail). Training sites are underlined, the others are validation sites.

Site	Observed H_2	Predicted H_2	Simulated $H_{2(0.01)}$	Simulated $H_{2(0.02)}$	Simulated $H_{2(0.05)}$
<u>AW</u>	25.2 ± 0.5	25.0 ± 0.6	23.8 ± 0.6	22.4 ± 0.6	19.0 ± 0.6
<u>Gr*</u>	19.6 ± 0.4	20.2 ± 0.0	21.2 ± 0.4	22.8 ± 0.4	25.5 ± 0.4
<u>Me</u>	23.4 ± 0.6	23.3 ± 0.4	22.1 ± 0.4	20.8 ± 0.4	17.2 ± 0.4
<u>Mo</u>	24.5 ± 0.6	24.3 ± 0.5	23.3 ± 0.5	22.0 ± 0.5	18.4 ± 0.5
<u>Tr</u>	23.8 ± 0.4	24.3 ± 0.8	23.1 ± 0.8	21.9 ± 0.8	18.2 ± 0.8
Au*	22.3 ± 1.6	20.3 ± 0.1	21.4 ± 0.1	23.0 ± 0.1	25.7 ± 0.1
Br	21.7 ± 0.8	22.5 ± 0.5	21.26 ± 0.5	20.0 ± 0.5	16.4 ± 0.5
Gl	25.8 ± 0.4	24.0 ± 0.1	22.8 ± 0.1	21.6 ± 0.1	17.9 ± 0.1
He	27.8 ± 1.4	23.3 ± 1.6	22.1 ± 1.6	20.9 ± 1.6	17.3 ± 1.6
Ml*	22.3 ± 0.8	21.8 ± 0.0	23.0 ± 0.0	24.6 ± 0.0	27.2 ± 0.0